Journal of Power Sources 252 (2014) 169–175

Contents lists available at ScienceDirect

Journal of Power Sources

journal homepage: www.elsevier.com/locate/jpowsour

Synthesis and characterization of high capacity Li_2MnSiO_4/C cathode material for lithium-ion battery

Long Qu [a], Shaohua Fang [a,*], Li Yang [a,b,*], Shin-ichi Hirano [b]

[a] School of Chemistry and Chemical Engineering, Shanghai Jiao Tong University, Shanghai 200240, China
[b] Hirano Institute for Materials Innovation, Shanghai Jiao Tong University, Shanghai 200240, China

HIGHLIGHTS

- Pure-phased Li_2MnSiO_4/C is prepared by sol–gel method with Mn_3O_4 nanoparticle.
- It owns nano-sized active material particle with 20–30 nm.
- It delivers an initial discharge capacity of 240 mAh g^{-1} at room temperature.
- Irreversible distortion might mainly effect on the cycle performance of Li_2MnSiO_4/C.

ARTICLE INFO

Article history:
Received 30 August 2013
Received in revised form
7 November 2013
Accepted 23 November 2013
Available online 1 December 2013

Keywords:
Lithium-ion battery
Cathode materials
Lithium manganese silicate
Manganous-manganic oxide nanoparticle

ABSTRACT

Li_2MnSiO_4/C composite is prepared by sol–gel method with Mn_3O_4 nanoparticle, and its carbon content, structure, and morphology are characterized. The results show that Li_2MnSiO_4/C exhibits pure phase with orthorhombic structure and the size of Li_2MnSiO_4 (20–30 nm) is smaller than Mn_3O_4 nanoparticle. As the cathode material of lithium-ion battery, Li_2MnSiO_4/C delivers an initial discharge capacity of about 240 mAh g^{-1} at the current density of 8 mA g^{-1}, corresponding to 1.44 mol of Li^+ per formula unit. The cycle performance of Li_2MnSiO_4/C at different current densities from 8 mA g^{-1}–320 mA g^{-1} is studied, and it is found that the capacity retention is improved with the increasing of current density. Basing on the results of ex-situ X-ray diffraction measurement, it is inferred that low degree of irreversible distortion for Li_2MnSiO_4 may result in the improved capacity retention at high current density.

1. Introduction

Polyanion-type compounds containing $(XO_4)^{n-}$ group as cathode materials of lithium-ion battery have lower exothermicity and higher safety, compared with lithium transition-metal oxides such as $LiMn_2O_4$, $LiCoO_2$, and $Li[Ni,Co,Mn]O_2$ [1–3]. Among the polyanion compounds, lithium transition-metal orthosilicates (Li_2MSiO_4, M = Fe or Mn) have been considered as the promising cathode materials of lithium-ion battery for electric vehicles, due to their high theoretical capacities (>300 mAh g^{-1}), low materials costs, and environmental friendliness [4–8]. Especially, Li_2MnSiO_4 has shown potential of high discharge capacity, and many research interests have been focused on Li_2MnSiO_4 cathode material [9–30].

Li_2MnSiO_4 suffers from low electronic conductivity and slow lithium-ion diffusion, which can be overcome by coating it with carbon and decreasing its particle size to nano-scale [31–33]. Up to now, sol–gel method has usually been applied on preparation of Li_2MnSiO_4/C with small particle size. Dominko et al. have firstly synthesized Li_2MnSiO_4/C by sol–gel method with CH_3COOLi, $(CH_3COO)_2Mn$, and nano-SiO_2, but the product contains the impurities of MnO and Li_2SiO_3 [5]. If nano-SiO_2 is replaced by soluble silicane, such as tetraethyl orthosilicate (TEOS), molecular-level mixing of Li, Mn and Si elements can be achieved during sol–gel process. Representatively, pure-phased Li_2MnSiO_4/C has been prepared by common sol–gel or microwave-solvothermal methods with soluble Li, Mn, and Si sources, and this kind of cathode at room temperature can deliver the initial discharge capacity higher than 200 mAh g^{-1} at low current density and show quick capacity degradation [6,34]. By using adipic acid as chelating agent of sol–gel method and carbon source, the capacity retention of Li_2MnSiO_4/C can be improved, but it only delivers the initial discharge capacity of less than 160 mAh g^{-1} and the discharge plateau can't be

* Corresponding authors. School of Chemistry and Chemical Engineering, Shanghai Jiao Tong University, Shanghai 200240, China. Tel.: +86 21 54748917; fax: +86 21 54741297.
E-mail addresses: housefang@sjtu.edu.cn (S. Fang), liyangce@sjtu.edu.cn (L. Yang).

0378-7753/$ – see front matter © 2013 Elsevier B.V. All rights reserved.
http://dx.doi.org/10.1016/j.jpowsour.2013.11.076

observed obviously as well [10,28]. Furthermore, Li_2MnSiO_4 with particle size of 15–20 nm has been directly synthesized by supercritical fluid method, and poly(3,4-ethylenedioxythiophene)-coated Li_2MnSiO_4 cathode can deliver an initial discharge capacity of 313 mAh g^{-1} (close to 2 mol of Li^+ per formula unit) at 40 °C [16].

For silicates cathode materials, nonideal cycle stability has prevented them from further applications, and some efforts have been taken to discover the factors determining their cycle performances [31,35–39]. Li_xPF_y, LiF and Li_2SiF_6 species have been detected on the cathode surfaces after cycle test in the case of Li_2FeSiO_4/C, and it is inferred that capacity degradation might result from the side reaction between Li_2FeSiO_4 and HF formed in the hydrolysis of $LiPF_6$-based electrolyte [35,37]. For $LiMn_2O_4$, $LiCoO_2$ and Li[Ni,Co,Mn]O_2 cathodes, this effect can cause transition-metal to dissolve into electrolyte [40–42]. Li_2MnSiO_4/C has poor capacity retention compared with Li_2FeSiO_4/C. Besides Mn dissolution, irreversible distortion of structure has been considered as another factor to result in quick capacity degradation of Li_2MnSiO_4/C, and Li_2MnSiO_4/C can transfer from crystalline state to amorphous state during the initial charge process at C/200 rate [39]. Furthermore, it is discovered that the cycle performances of Li_2FeSiO_4/C and Li_2MnSiO_4/C can be obviously improved with the increasing of charge–discharge rate or current density [7,11,19,20,43,44], but until now no research work has tried to explain this phenomenon deeply.

In this work, we prepared pure-phased Li_2MnSiO_4/C by sol–gel method with Mn_3O_4 nanoparticle. And it was found that this Li_2MnSiO_4/C delivered an initial discharge capacity of about 240 mAh g^{-1} at the current density of 8 mA g^{-1} at room temperature, and it had better cycle performance compared with other products of Li_2MnSiO_4/C which were prepared with soluble Mn source and showed the high initial discharge capacity at low current density (>200 mAh g^{-1}) [6,20,34]. After investigating Mn dissolution in electrolyte, impedance spectroscopy of cell and ex-situ X-ray diffraction pattern of cathode after the initial and 30th charge–discharge cycles, it was inferred that low degree of irreversible distortion for Li_2MnSiO_4 during every charge–discharge cycle at high current density, might result in the improved capacity retention at high current density.

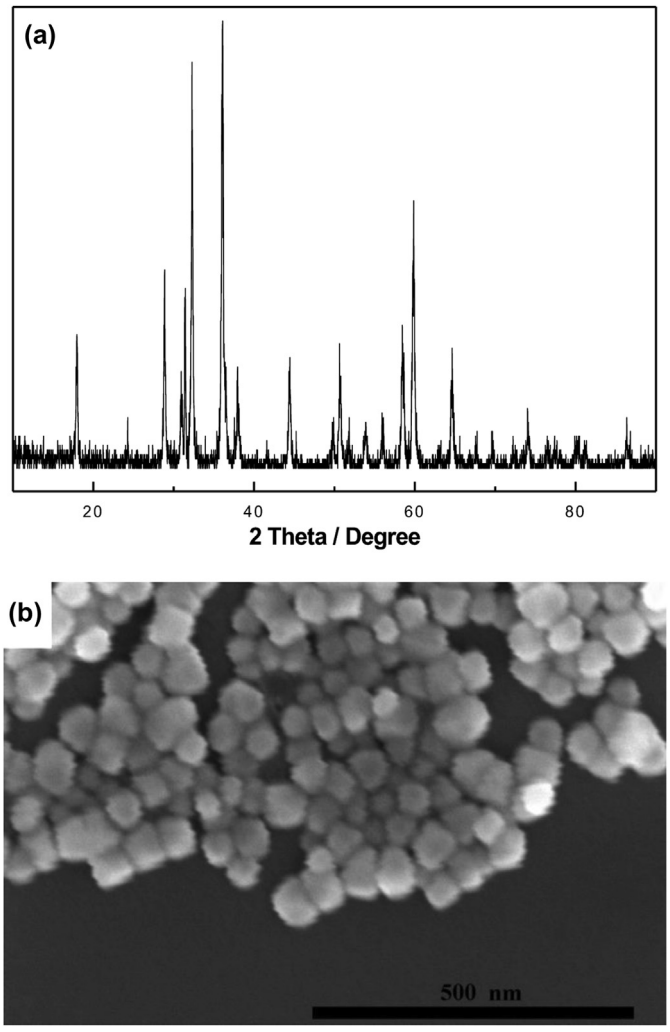

Fig. 1. (a) XRD pattern and (b) SEM image of Mn_3O_4.

2. Experimental

2.1. Preparation of Mn_3O_4 nanoparticle

All the reagents and solvents were analytical purity, and purchased from Sinopharm Chemical Reagent Co. Ltd., and used as received. Mn_3O_4 nanoparticle was synthesized by hydrothermal method as described in the literature [45]. Typically, $KMnO_4$ (0.500 g) was completely dissolved in deionized water (20 mL), PEG200 (60 mL) was then added to the solution and stirred to form a suspension. The mixture was poured into a Teflon-lined stainless steel autoclave (100 mL), which was subsequently sealed and maintained at 140 °C for 18 h. The brown precipitate was washed with water and ethanol several times, and it was dried at 60 °C for overnight.

2.2. Preparation of Li_2MnSiO_4/C composite

The Li_2MnSiO_4/C composite was synthesized by sol–gel method. Typically, $LiCH_3COO{\cdot}2H_2O$ (2.040 g), as-prepared Mn_3O_4 nanoparticle (0.763 g), and TEOS (2.083 g) were dispersed in water–ethanol (1:10 V/V), and CH_3COOH was added as a catalyst. The mixture was treated with ultrasonic bath at 85 °C for at least 2 h to prevent Mn_3O_4 nanoparticles from agglomerating, and then stirred by mechanical stirring and refluxed at 85 °C for at least 36 h. The solvents were evaporated slowly at 80 °C, and the powder was grinded by ball-milling with adding sucrose and acetone at least for 8 h. After evaporating the acetone, the dry powder was calcined in a horizontal quartz tube oven flowing argon atmosphere at 700 °C for 10 h to obtain the Li_2MnSiO_4/C, and the product was then transferred to glove-box.

2.3. Materials characterization

X-ray diffraction (XRD) characterizations of the samples were carried out with a Rigaku D/max-2200 PC diffractometer and filtered Cu Kα radiation operated at 40 kV and 20 mA. Scanning electron microscope (SEM) and transmission electron microscope (TEM) characterizations were carried out with a NOVA NanoSEM 230 and JEOL JEM-2010HT, respectively. The amount of carbon in Li_2MnSiO_4/C was measured by using a Shanghai Baoying Photoelectric Technology CS-206 high frequency carbon–sulfur infrared analyzer (CSI), and the value was about 16 wt %.

2.4. Electrode preparation and electrochemical measurements

The electrochemical performances of Li_2MnSiO_4/C composite were assessed using CR-2016 coin cells. The cathode was prepared by mixing 80 wt % of Li_2MnSiO_4/C with 10 wt % acetylene black and

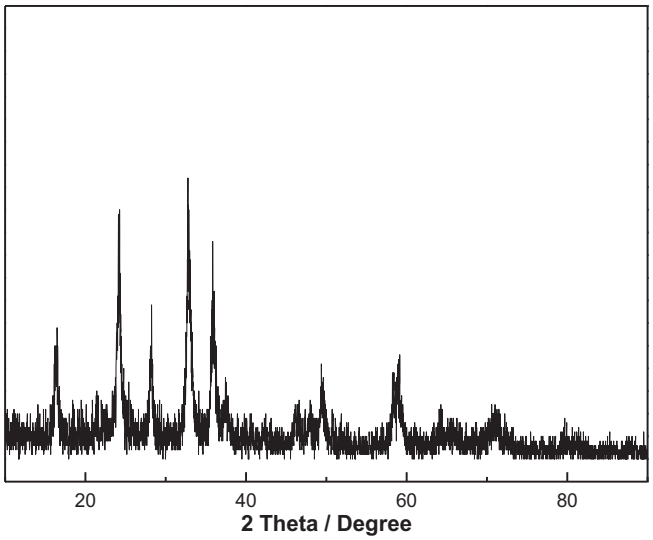

Fig. 2. XRD pattern of Li_2MnSiO_4/C.

10 wt % PVDF (firstly dissolved in N-methyl-2-pyrrolidene). The electrode was formed by coating the slurry onto Al foils after drying overnight at 110 °C in a vacuum oven, and the typical cathode loading was 1–2 mg cm^{-2}. The cells fabrication were carried out in a glove-box (Braun, Master 100 Lab) full-filled with argon atmosphere, and the cells were assembled with the Li_2MnSiO_4/C cathode, Li metal anode, glass fiber (Whatman GF/A) separator, and 1 M $LiPF_6$ in ethylene carbonate (EC) and dimethyl carbonate (DMC) (1:1 by weight ratio). The amounts of electrolyte used in the cells were weighted. The cells were assessed by galvanostatic charge–discharge measurements executing between 1.5 and 4.8 V at room temperature in a Land CT 2001 battery test system, and all reported capacity values were quoted with respect to the mass of the Li_2MnSiO_4. Electrochemical impedance spectroscopy (EIS) of coin cell was measured by using a CHI 604b electrochemistry workstation (0.1 Hz–100 kHz, applied voltage 5 mV).

2.5. Manganese dissolution and ex-situ XRD measurements

The coin cells were carefully disassembled in glove-box after certain charge–discharge cycles at different current densities, and all the parts were washed with DMC, and the liquid parts were then examined by an inductively coupled plasma analyzer (ICP, Thermo iCAP6300) to determine the concentration of Mn in the electrolyte. The cathodes were characterized by XRD after drying at room temperature in vacuum for 8 h.

3. Results and discussions

According to Fig. 1a, the XRD pattern was indexed to Mn_3O_4 (JCPDS 24-0734), and it indicated that the Mn source used in this experiment was Mn_3O_4. As shown in Fig. 1b, the SEM image of Mn_3O_4 showed that the particle size was estimated to be in the range from 50 to 80 nm.

Fig. 2 showed the XRD pattern of Li_2MnSiO_4/C, and all the reflections were in accord with the reported results and indexed to orthorhombic structure with space group $Pmn2_1$ [5,6,27]. No manganese oxides, lithium silicates, manganese silicates or other impurities phases were observed for Li_2MnSiO_4/C. Carbon was generated from the carbonization of sucrose, and its diffraction peaks were not detected due to its amorphous state. The XRD pattern suggested that the Mn_3O_4 nanoparticles reacted with Li and Si sources under the reduction of carbon to produce the Li_2MnSiO_4 during the process of calcination, and the presence of carbon didn't prevent from this reaction to result in some impurities of manganese oxides and lithium silicates in the final product. Usually, soluble Li, Si, and transition-metal (Fe or Mn) sources could be used to synthesize pure-phased Li_2MSiO_4/C (M = Fe or Mn) by sol–gel method, because the sources were easy to obtain the gel with uniform distribution of Li, Si, and transition-metal (Fe or Mn) atoms. In our previous work, it was found that pure-phased Li_2FeSiO_4/C could be prepared by sol–gel method with Fe_2O_3 particle to replace soluble Fe source [7,8]. Here, pure-phased Li_2MnSiO_4/C could also be prepared by the similar strategy, and it further proved that replacing soluble metal source by metal oxide in sol–

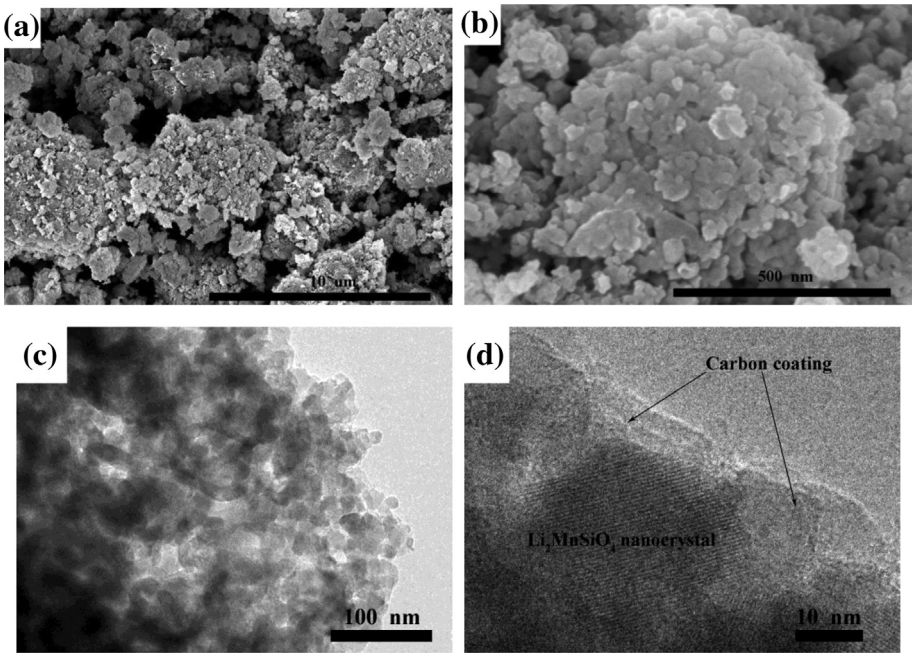

Fig. 3. SEM images of Li_2MnSiO_4/C at (a) low and (b) high magnification, (c) TEM and (d) high-resolution TEM images of Li_2MnSiO_4/C.

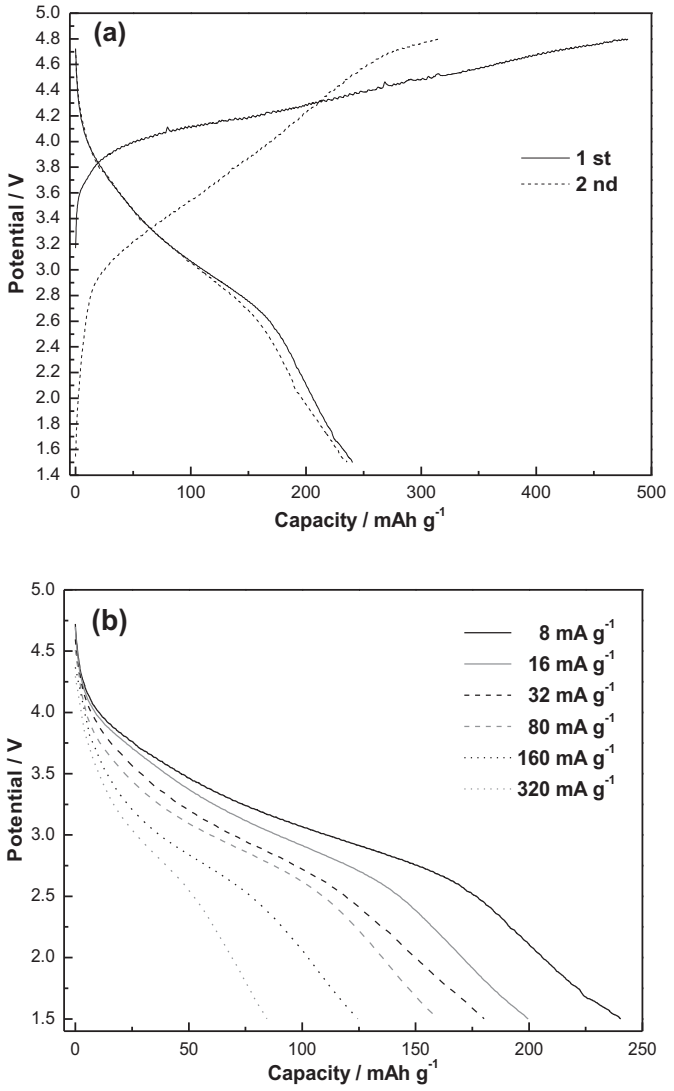

Fig. 4. (a) The initial and second charge–discharge profiles of Li_2MnSiO_4/C at the current density of 8 mA g^{-1} and (b) the initial discharge profiles of Li_2MnSiO_4/C at different current densities.

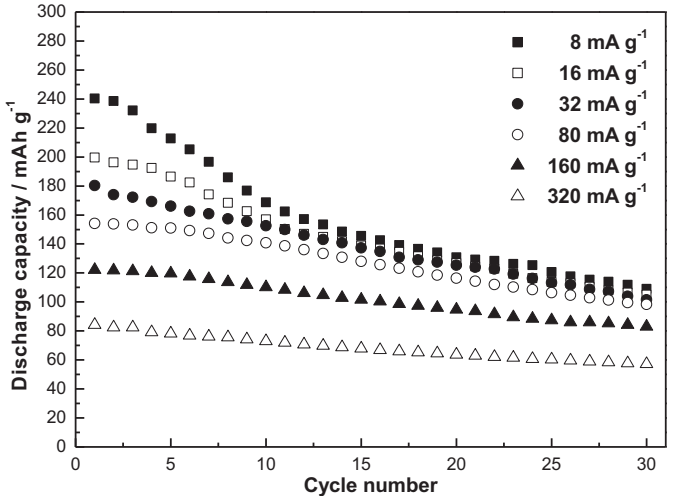

Fig. 5. Cycle performances of Li_2MnSiO_4/C composite cathode at different current densities for 30 cycles.

gel process was another general pathway to prepare pure-phased Li_2MSiO_4/C cathode materials.

SEM images of Li_2MnSiO_4/C composite were shown in Fig. 3a and b. Fig. 3a showed that Li_2MnSiO_4/C exhibited the irregular shape with micro-sized particles. According to the magnified SEM image (Fig. 3b), it was apparent that the micro-sized particles formed by a tight accumulation of nanoparticles. TEM measurement was used to further investigate the particle size of Li_2MnSiO_4 and the carbon coating, and the images were shown in Fig. 3c and d. It could be found from Fig. 3c that Li_2MnSiO_4 particles were embedded into amorphous carbon, and its size ranged from 20 to 30 nm, which was close to those Li_2MnSiO_4/C prepared with soluble Li, Si and Mn sources [6,20,34]. High-resolution TEM image in Fig. 3d revealed that Li_2MnSiO_4 nanocrystal was wrapped by carbon layer with thickness of several nanometers. In our previous work, when 500 nm Fe_2O_3 microsphere and 50 nm Fe_2O_3 particle were used, the size of Li_2FeSiO_4 was close to Fe_2O_3, and it was inferred that the size of Li_2FeSiO_4 could be controlled with the size of Fe_2O_3 particle by using simple sol–gel method [7,8]. Here, the size of Li_2MnSiO_4 was smaller than Mn_3O_4 nanoparticle (Fig. 1b), and it indicated that the particle might fragment gradually during the process of Li_2MnSiO_4 forming. In the other words, the size of Li_2MnSiO_4 could not be controlled by using Mn_3O_4 particle as a template.

Galvanostatic charge–discharge measurements were carried out at room temperature to assess electrochemical performances of Li_2MnSiO_4/C composite as cathode. Fig. 4a showed the initial and second charge–discharge profiles at the current density of 8 mA g^{-1}. The second charge plateau was obviously lower than the initial one, which suggested that a structural rearrangement might occur during the initial charge process [46]. This Li_2MnSiO_4/C composite delivered an initial discharge capacity of about 240 mAh g^{-1}, corresponding to 1.44 mol of Li^+ per formula unit. Compared with the Li_2MnSiO_4/C prepared by sol–gel method with soluble Li, Si and Mn sources, this initial discharge capacity at low current density was higher than two products (209 mAh g^{-1} at 30 °C [6], and 225 mAh g^{-1} at 25 °C [34]), and slightly lower than one product reported recently (253 mAh g^{-1} at 25 °C [20]). Fig. 4b showed the initial discharge profiles of Li_2MnSiO_4/C at different current densities, and the discharge capacities decreased with the increasing current densities. For example, when the current density increased to 160 mA g^{-1}, the initial discharge capacity was about 125 mAh g^{-1}, which was 52% of the capacity at the current density of 8 mA g^{-1}.

Fig. 5 showed the cycle performances of Li_2MnSiO_4/C composite cathode at different current densities for 30 cycles, and the corresponding capacity retentions were listed in Table 1. The discharge capacities at different current densities gradually declined with the increasing cycle number, and the capacity retention was improved with the increasing current density. For instance, the discharge capacities decayed to 109 mAh g^{-1} at the current density of 8 mA g^{-1} after 30 cycles, and only about 45% of its initial capacity

Table 1
The concentration of manganese in electrolyte at different current densities after the initial and 30th cycles, and the corresponding capacity retentions.

Current density (mA g^{-1})	Capacity retention (%)	Mn concentration after the initial cycle (ppm)	Mn concentration after the 30th cycle (ppm)
8	45.4	69.6	108.1
16	52.6	60.8	92.8
32	56.3	30.9	72.6
80	63.7	24.8	70.9
160	67.9	23.5	67.4
320	68.0	11.1	60.3

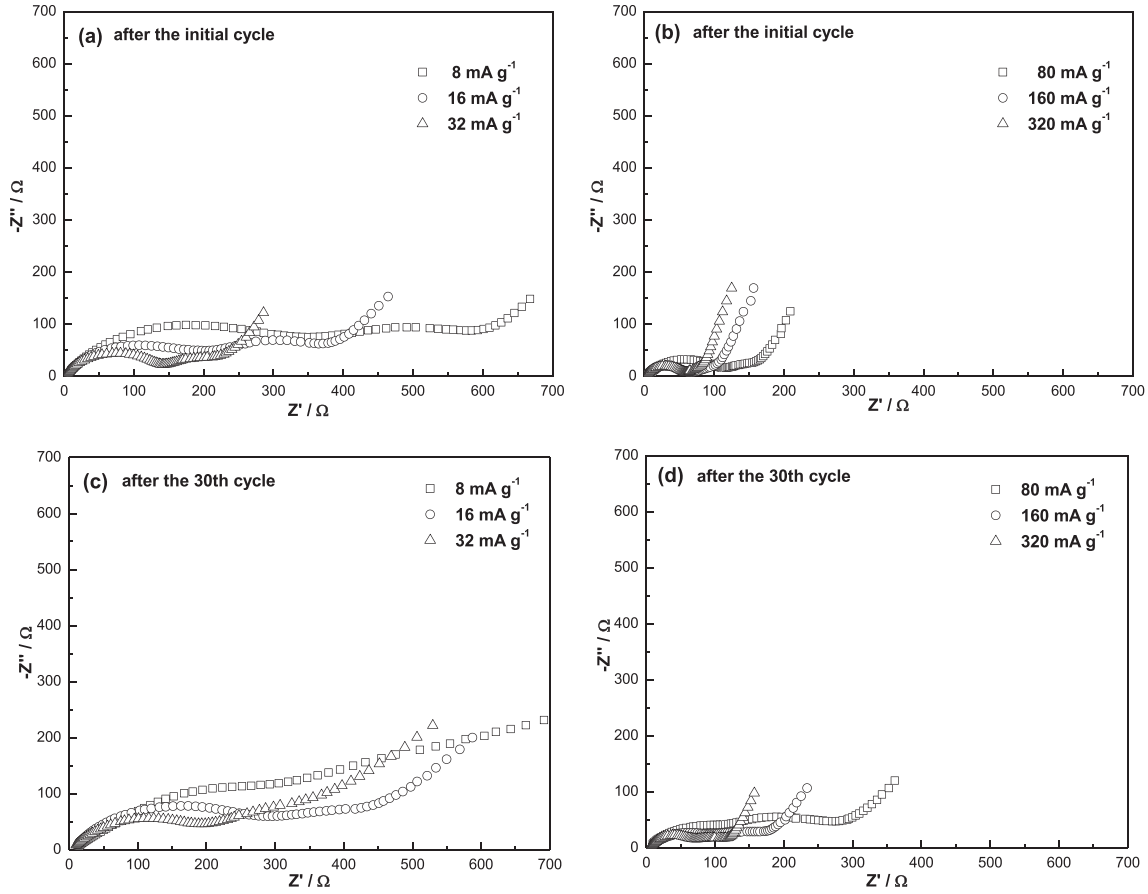

Fig. 6. Impedance response for Li_2MnSiO_4/C cathode in the cells after the initial and 30th cycles at different current densities: (a) 8 mA g^{-1}, 16 mA g^{-1} and 32 mA g^{-1} after the initial cycle, (b) 80 mA g^{-1}, 160 mA g^{-1} and 320 mA g^{-1} after the initial cycle, (c) 8 mA g^{-1}, 16 mA g^{-1} and 32 mA g^{-1} after the 30th cycle and (d) 80 mA g^{-1}, 160 mA g^{-1} and 320 mA g^{-1} after the 30th cycle.

was retained. While the current density increased from 8 to 320 mA g^{-1}, the capacity retention of 30 cycles was improved from 45.4% to 68.0%. Compared with three products of pure-phased Li_2MnSiO_4/C which were prepared by sol–gel method with soluble Mn source and showed the high initial discharge capacity at low current density (>200 mAh g^{-1}) [6,20,34], this cathode prepared with Mn_3O_4 as Mn source had better cycle performance. Combining with our previous finding that Li_2FeSiO_4/C cathode prepared with Fe_2O_3 as Fe source also had better cycle performance [7,8], it indicated that replacing soluble metal source by metal oxide in sol–gel process was helpful to improve cycle performance of silicate cathode material, which might result from more compact coating of carbon on the cathode and more effective restraining the side reaction between the cathode and HF formed in the hydrolysis of $LiPF_6$-based electrolyte.

The concentrations of Mn in electrolyte after the initial and 30th cycles at different current densities were listed in Table 1. After the initial cycle, Mn dissolution gradually decreased with the increasing current density. The concentration of Mn in electrolyte was 69.6 ppm at the current density of 8 mA g^{-1}, and it reduced to 11.1 ppm while current density increased from 8 mA g^{-1}–320 mA g^{-1}, which was about 16% of the value at the current density of 8 mA g^{-1}. After the 30th cycle, all the concentrations of Mn in electrolyte at different current densities were larger than the corresponding values after the initial cycle, but the increasing rate of Mn concentration was different for each current density. For instance, the concentration of Mn in electrolyte at the current density of 8 mA g^{-1} was 108.1 ppm after the 30th cycle, which went up by 55% as against the value after the initial cycle. And the concentration of Mn at the current density of 320 mA g^{-1} was 60.3 ppm after the 30th cycle, which went up by more than 4 times as against the value after the initial cycle. Although the concentration of Mn at the current density of 8 mA g^{-1} was still the highest in the samples after 30 cycles, the gap between it and the values at other current densities became smaller. In the other words, when the current density was higher, the increasing of Mn concentration was quicker during the process from the second cycle to the 30th cycle. The Mn dissolution might be caused by reaction of Li_2MnSiO_4 cathode with HF generated from the hydrolysis of $LiPF_6$-based electrolyte [42]. During the initial cycle, when cell was tested at lower current density, charging process can be maintained for a long time in high potential, where the side reactions between the fresh surface of Li_2MnSiO_4 and electrolyte were intensive. Therefore the Mn concentration at low current density was high after the initial cycle. Meanwhile, a certain surface film might also be generated on the cathode after the initial cycle, and the surface film formed at low current density could be more beneficial to protect the cathode from the corrosive reaction of electrolyte during the subsequent charge–discharge cycles, which could cause the slow increasing of Mn concentration at low current density. Furthermore, after considering that the capacity retention was improved with the increasing current density, it was also inferred that the Mn dissolution might not be the main factor to result in the poor capacity retention of Li_2MnSiO_4 cathode at low current density.

Fig. 6 showed the impedance responses after the initial and 30th cycles at different current densities. Two semicircles in high-

frequency and medium-frequency regions could be assigned to surface film resistance (R_{sf}) and charge transfer resistance (R_{ct}), respectively [47]. As shown in Fig. 6a and b, R_{sf} and R_{ct} gradually decreased with the increasing current density after the initial cycle. When the current density increased to 320 mA g^{-1}, R_{ct} had reduced to be unobvious. It was found from Fig. 6c and d that R_{sf} and R_{ct} still decreased with the increasing current density after 30 cycles. All of the R_{sf} at the different current densities after the 30th cycle were bigger than the corresponding values after the initial cycle. The results of impedance response meant that the surface film on cathode changed with the current density and cycle number. And they also further proved that it was possible that the surface film formed at low current density could be more beneficial to protect the cathode from the corrosive reaction of electrolyte.

Ex-situ XRD measurement was used to investigate the changing of Li_2MnSiO_4 structure at different current densities after charge–discharge cycles, and the results were shown in Fig. 7. It was observed from Fig. 7a that the diffraction peaks of Li_2MnSiO_4 at the current densities of 8 mA g^{-1}, 16 mA g^{-1} and 32 mA g^{-1} disappeared after the initial cycle, and it indicated that the crystalline Li_2MnSiO_4 turned into an amorphous state due to the irreversible distortion of structure during the charge process [39]. Interestingly, the diffraction peaks of Li_2MnSiO_4 at the current densities of 80 mA g^{-1}, 160 mA g^{-1} and 320 mA g^{-1} could still be observed after the initial cycle, and peak intensity at the current density of 320 mA g^{-1} was the strongest among three patterns. The results were similar to how the XRD patterns of Li_2MnSiO_4 changed during the initial cycle at low current density after charging to different voltages or extracting different amounts of Li [6,39]. It indicated that when cell charged at high current density, the internal resistance of cell caused factual cut-off voltage to be lower than 4.8 V, and Li had been extracted from part of crystalline Li_2MnSiO_4. So the residual part without being delithiated could still make the diffraction peaks of crystalline Li_2MnSiO_4. As shown in Fig. 7b, the diffraction peaks of Li_2MnSiO_4/C at the current densities from 8 to 160 mA g^{-1} had not been observed after 30 cycles, and the diffraction peaks at the current density of 320 mA g^{-1} still existed, which intensity was weaker than the peak intensity after the initial cycle. Hence, it was concluded that low degree of irreversible distortion for Li_2MnSiO_4 during every charge–discharge cycle at high current density, might be the main factor to result in the improved capacity retention of Li_2MnSiO_4 cathode at high current density. Furthermore, one peak at $2\theta = 38^\circ$ was observed for different current densities after the initial cycle, and it might be corresponding to the products from the changing of Li_2MnSiO_4 structure.

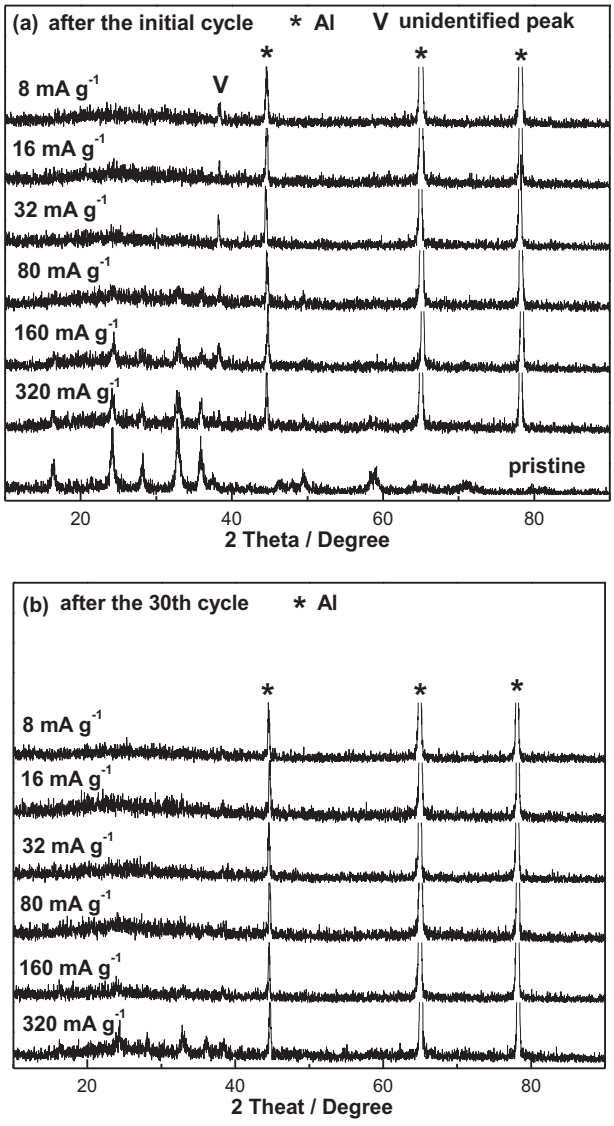

Fig. 7. Ex-situ XRD patterns of Li_2MnSiO_4/C at different current densities after (a) the initial cycle and (b) the 30th cycle.

4. Conclusions

Li_2MnSiO_4/C composite was successfully synthesized with Mn_3O_4 nanoparticle by sol–gel method, and it was used as cathode material of lithium-ion battery. It was found that the sample owned pure phase with orthorhombic structure and nano-sized active material particle with 20–30 nm. The Li_2MnSiO_4/C cathode delivered an initial discharge capacity as high as 240 mAh g^{-1} at the current density of 8 mA g^{-1} at room temperature, corresponding to 1.44 mol of Li^+ per formula unit. By investigating Mn dissolution in electrolyte, impedance spectroscopy of cell and ex-situ XRD pattern of cathode after the initial and 30th charge–discharge cycles, it was inferred that the degree of irreversible distortion for Li_2MnSiO_4 might mainly determine the capacity retentions at different current densities.

Acknowledgments

The financial supports from the National Natural Science Foundation of China (grants no. 21103108, 21173148 and 21373136) are gratefully acknowledged. We thank the Instrumental Analysis Center of Shanghai Jiao Tong University for Materials Characterization.

References

[1] M.S. Whittingham, Chem. Rev. 104 (2004) 4271–4302.
[2] J.W. Fergus, J. Power Sources 195 (2010) 939–954.
[3] A.K. Padhi, K.S. Nanjundaswamy, J.B. Goodenough, J. Electrochem. Soc. 144 (1997) 1188–1194.
[4] A. Nytén, A. Abouimrane, M. Armand, T. Gustafsson, J.O. Thomas, Electrochem. Commun. 7 (2005) 156–160.
[5] R. Dominko, M. Bele, M. Gaberšček, A. Meden, M. Remškar, J. Jamnik, Electrochem. Commun. 8 (2006) 217–222.
[6] Y.-X. Li, Z.-L. Gong, Y. Yang, J. Power Sources 174 (2007) 528–532.
[7] L. Qu, S. Fang, L. Yang, S.-i. Hirano, J. Power Sources 217 (2012) 243–247.
[8] L. Qu, S. Fang, Z. Zhang, L. Yang, S.-i. Hirano, Mater. Lett. 108 (2013) 1–4.
[9] S. Aono, T. Tsurudo, K. Urita, I. Moriguchi, Chem. Commun. 49 (2013) 2939–2941.
[10] V. Aravindan, K. Karthikeyan, S. Ravi, S. Amaresh, W.S. Kim, Y.S. Lee, J. Mater. Chem. 20 (2010) 7340–7343.
[11] A. Bhaskar, M. Deepa, T.N. Rao, U.V. Varadaraju, J. Electrochem. Soc. 159 (2012) A1954–A1960.

[12] S. Choi, S.J. Kim, Y.J. Yun, S.S. Lee, S.-Y. Choi, H.-K. Jung, Mater. Lett. 105 (2013) 113–116.
[13] S. Devaraj, M. Kuezma, C.T. Ng, P. Balaya, Electrochim. Acta 102 (2013) 290–298.
[14] P. Ghosh, S. Mahanty, R.N. Basu, J. Electrochem. Soc. 156 (2009) A677–A681.
[15] T. Kawase, H. Yoshitake, Microporous Mesoporous Mater. 155 (2012) 99–105.
[16] D.M. Kempaiah, D. Rangappa, I. Honma, Chem. Commun. 48 (2012) 2698–2700.
[17] A. Kojima, T. Kojima, M. Tabuchi, T. Sakai, J. Electrochem. Soc. 159 (2012) A532–A537.
[18] M. Kuezma, S. Devaraj, P. Balaya, J. Mater. Chem. 22 (2012) 21279–21284.
[19] J. Liu, H. Xu, X. Jiang, J. Yang, Y. Qian, J. Power Sources 231 (2013) 39–43.
[20] S. Liu, J. Xu, D. Li, Y. Hu, X. Liu, K. Xie, J. Power Sources 232 (2013) 258–263.
[21] W. Liu, Y. Xu, R. Yang, J. Alloys Compd. 480 (2009) L1–L4.
[22] F. Wang, J. Chen, C. Wang, B. Yi, J. Electroanal. Chem. 688 (2013) 123–129.
[23] Q. Zhang, Q. Zhuang, S. Xu, X. Qiu, Y. Cui, Y. Shi, Y. Qiang, Ionics 18 (2011) 487–494.
[24] S. Zhang, C. Deng, F.L. Liu, Q. Wu, M. Zhang, F.L. Meng, H. Gao, J. Electroanal. Chem. 689 (2013) 88–95.
[25] S. Zhang, Z. Lin, L. Ji, Y. Li, G. Xu, L. Xue, S. Li, Y. Lu, O. Toprakci, X. Zhang, J. Mater. Chem. 22 (2012) 14661–14666.
[26] Y. Zhao, C. Wu, J. Li, L. Guan, J. Mater. Chem. A 1 (2013) 3856–3859.
[27] C. Deng, S. Zhang, B.L. Fu, S.Y. Yang, L. Ma, Mater. Chem. Phys. 120 (2010) 14–17.
[28] V. Aravindan, K. Karthikeyan, S. Amaresh, Y.S. Lee, Electrochem. Solid-State Lett. 14 (2011) A33–A35.
[29] D. Rangappa, K.D. Murukanahally, T. Tomai, A. Unemoto, I. Honma, Nano Lett. 12 (2012) 1146–1151.
[30] M.K. Devaraju, T. Tomai, A. Unemoto, I. Honma, RSC Adv. 3 (2013) 608–615.
[31] R. Dominko, J. Power Sources 184 (2008) 462–468.
[32] S.Y. Chung, J.T. Bloking, Y.M. Chiang, Nat. Mater. 1 (2002) 123–128.
[33] V. Aravindan, K. Karthikeyan, K.S. Kang, W.S. Yoon, W.S. Kim, Y.S. Lee, J. Mater. Chem. 21 (2011) 2470–2475.
[34] T. Muraliganth, K.R. Stroukoff, A. Manthiram, Chem. Mater. 22 (2010) 5754–5761.
[35] C. Dippel, S. Krueger, R. Kloepsch, P. Niehoff, B. Hoffmann, S. Nowak, S. Passerini, M. Winter, J. Li, Electrochim. Acta 85 (2012) 66–71.
[36] R. Dominko, I. Arčon, A. Kodre, D. Hanžel, M. Gaberšček, J. Power Sources 189 (2009) 51–58.
[37] D. Ensling, M. Stjerndahl, A. Nytén, T. Gustafsson, J.O. Thomas, J. Mater. Chem. 19 (2009) 82–88.
[38] A. Nyten, M. Stjerndahl, H. Rensmo, H. Siegbahn, M. Armand, T. Gustafsson, K. Edstrom, J.O. Thomas, J. Mater. Chem. 16 (2006) 3483–3488.
[39] R. Dominko, M. Bele, A. Kokalj, M. Gaberscek, J. Jamnik, J. Power Sources 174 (2007) 457–461.
[40] G.G. Amatucci, J.M. Tarascon, L.C. Klein, Solid State Ionics 83 (1996) 167–173.
[41] S.B. Jang, S.H. Kang, K. Amine, Y.C. Bae, Y.K. Sun, Electrochim. Acta 50 (2005) 4168–4173.
[42] H.-C. Wang, C.-H. Lu, J. Power Sources 119–121 (2003) 738–742.
[43] J. Bai, Z. Gong, D. Lv, Y. Li, H. Zou, Y. Yang, J. Mater. Chem. 22 (2012) 12128–12132.
[44] Z. Zheng, Y. Wang, A. Zhang, T. Zhang, F. Cheng, Z. Tao, J. Chen, J. Power Sources 198 (2012) 229–235.
[45] Y. Li, H. Tan, X.Y. Yang, B. Goris, J. Verbeeck, S. Bals, P. Colson, R. Cloots, G. Van Tendeloo, B.L. Su, Small 7 (2011) 475–483.
[46] A. Nyten, S. Kamali, L. Haggstrom, T. Gustafsson, J.O. Thomas, J. Mater. Chem. 16 (2006) 2266–2272.
[47] Y.J. Kang, J.H. Kim, S.W. Lee, Y.K. Sun, Electrochim. Acta 50 (2005) 4784–4791.